The Astrophysical Journal, 665:799–804, 2007 August 10

MAGNETIC FIELD STRENGTH IN THE SOLAR CORONA FROM TYPE II BAND SPLITTING

K.-S. Cho,[1,2] J. Lee,[2] D. E. Gary,[2] Y.-J. Moon,[1] and Y. D. Park[1]

Received 2007 February 8; accepted 2007 April 12

ABSTRACT

The phenomenon of band splitting in type II bursts can be a unique diagnostic for the magnetic field in the corona, which is, however, inevitably sensitive to the ambient density. We apply this diagnostic to the CME-flare event on 2004 August 18, for which we are able to locate the propagation of the type II burst and determine the ambient coronal electron density by other means. We measure the width of the band splitting on a dynamic spectrum of the bursts observed with the Green Bank Solar Radio Burst Spectrometer (GBSRBS), and convert it to the Alfvén Mach number under the Rankine-Hugoniot relation. We then determine the Alfvén speed and magnetic field strength using the coronal background density and shock speed measured with the MLSO/MK4 coronameter. In this way we find that the shock compression ratio is in the range of 1.5–1.6, the Alfvénic Mach number is 1.4–1.5, the Alfvén speed is 550–400 km s^{-1}, and finally the magnetic field strength decreases from 1.3 to 0.4 G while the shock passes from 1.6 to 2.1 $R_\odot$. The magnetic field strength derived from the type II spectrum is finally compared with the potential field source surface (PFSS) model for further evaluation of this diagnostic.

Subject heading: Sun: coronal mass ejections (CMEs)

1. INTRODUCTION

The solar magnetic field plays an important role over the entire range of coronal heights. The magnetic field in the range of 1.1–3 $R_\odot$ is especially important as an interface between the photospheric magnetic field and the solar wind. Its structure and time-dependent change affects space weather by modifying solar wind conditions. Techniques for measuring the magnetic field in this height range are more limited than those for the magnetic fields in the lower coronal heights. First, the conventional Zeeman splitting technique employing infrared emission lines from Fe XIII is limited to the heights lower than 1.15 $R_\odot$ (Lin et al. 2000). Second, gyroresonance radiation in microwave and decimetric wavelengths work for strong magnetic fields above 100 G, and thus in the height range below 1.5 $R_\odot$ (White 2005). Third, the mode-coupling phenomenon (Cohen 1960) of microwave radiation can, in principle, detect the magnetic field in this high corona, but is subject to favorable viewing angles (Lee et al. 1998). Type II bursts that show the band-splitting feature can be used to determine the ambient magnetic field along the path of the shocks propagating through the solar corona (Smerd et al. 1975). It is metric type II bursts that correspond to this height range. If none of these observations are available, we can always rely on the coronal field extrapolation from the photospheric magnetic field. At this coronal height, the potential field source surface (PFSS) model (Schatten et al. 1969) can be used. Recently, a fair agreement between the field line topology predicted by the PFSS model and the coronal loops seen in EUV and soft X-ray images was found (Schrijver & DeRosa 2003). However, it is still unknown to what extent it can reproduce the coronal field *strength*. In this paper, we will apply the band-splitting technique to the data of a metric type II burst and compare the result with the corresponding PFSS model.

The band-splitting technique works as follows. A type II burst itself is a unique diagnostic for density in the shock front, as it appears as two drifting bands in radio dynamic spectrum due to plasma emission at the fundamental and harmonic of local plasma frequency at the shock front (Nelson & Melrose 1985). It can provide magnetic field information when it shows splitting of emission bands. The band splitting is not seen in every type II burst, and the mechanism is still not fully understood. One plausible theory is that the band splitting appears as the plasma emission occurs from both upstream (Smith 1971) and downstream (Tidman 1965; Tidman et al. 1966) of the coronal shock front. Recent observational support for this theory was given by Vrsnak et al. (2001) through in situ measurements of shocks at 1 AU that show the upstream and downstream emissions (see their Fig. 4). Smerd et al. (1974, 1975) accepted this interpretation, and relate the spectral width of band splitting to the shock compression ratio, which then yields the Alfvénic Mach number, M_A, under the Rankine-Hugoniot jump relation. If information on the density and shock velocity are also available, we can finally determine the magnetic field at the shock front using these parameters. Smerd et al. (1974, 1975) applied this technique to nine type II bursts with band-splitting structures to find $1.2 \leq M_A \leq 1.7$ and $0.3\ \mathrm{G} \leq B \leq 4$ G. Later Vrsnak et al. (2002) applied the method to 18 metric type II bursts to find the coronal Alfvén speed in the range of 400–700 km s^{-1} and magnetic field in the range of 1–7 G at 1.6 $R_\odot$ and 0.3–0.9 G at 2.5 $R_\odot$.

As pointed out by Vrsnak et al. (2002), the result of the magnetic field derived from type II band splitting is sensitive to the adopted value of the coronal density. Other factors such as the shock angle and plasma β also affect the diagnostic, but the uncertainties associated with these parameters are much less than the one caused by the unknown density. Although Vrsnak et al. (2002) demonstrated this issue with various one-dimensional density models, we additionally note that the importance of density information in this diagnostic is not only as a factor in converting the Alfvén velocity to the magnetic field, but also in determining the shock speed from the type II frequencies. Namely, depending on which path is chosen for the shock propagated along in an inhomogeneous corona, the shock speed derived from the drift of type II bursts will differ. This in turn affects the derivation of the Alfvén speed from the given Mach number. This uncertainty associated with the shock location has not been studied before. What is new in this study is that we apply the band-splitting technique to an event where we were able

[1] Korea Astronomy and Space Science Institute, Whaamdong, Yooseong-ku, Daejeon 305-348, Korea; kscho@kasi.re.kr.

[2] Center for Solar-Terrestrial Research, New Jersey Institute of Technology, Newark, NJ 07102.

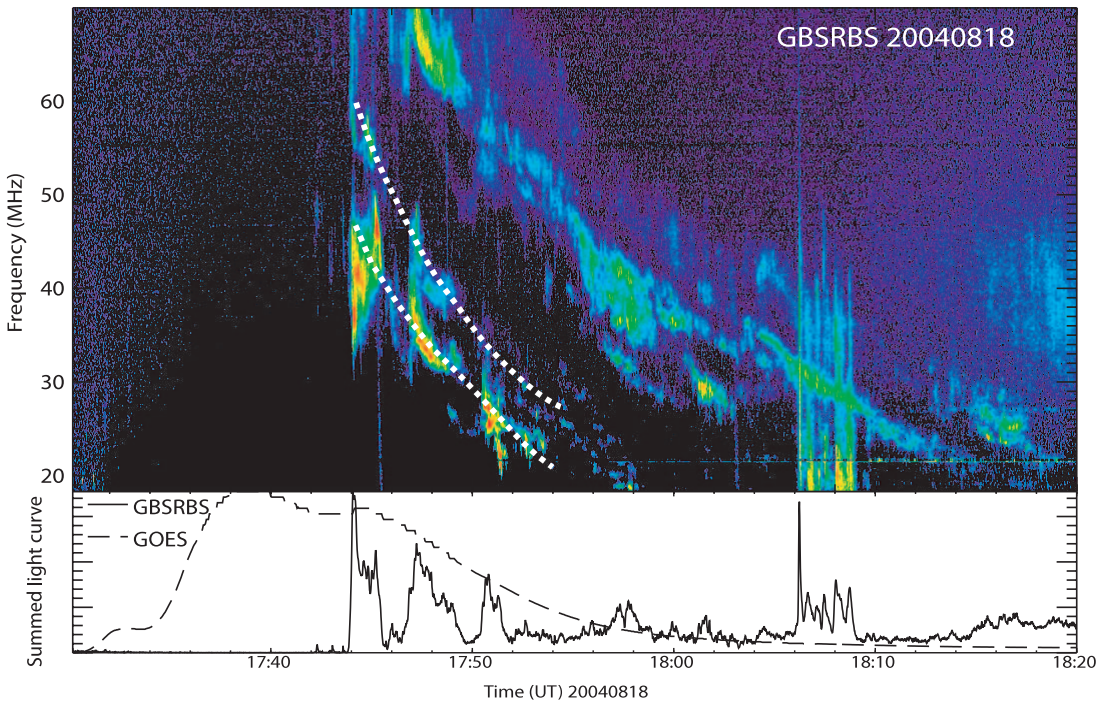

FIG. 1.—*Top*: Measurements of emission frequencies (*dotted lines*) at the upper (HFB) and lower (LFB) frequency branches in the fundamental band of the type II burst observed by GBSRBS. Dashed and solid lines in lower panel denote the *GOES* X-ray flux (0.5–4 Å) and total radio flux of GBSRBS from 18 to 70 MHz, respectively.

to locate the shock and provide the density information along the shock path. Since we are dealing with only a single event with detailed spatial information, we will focus on how such spatial information will affect the diagnostic as well as the resulting magnetic field itself.

2. EVENT DESCRIPTION

The type II burst occured on 2004 August 18. The associated coronal mass ejection (CME) was observed by the MLSO/MK4 coronameter (1.08–2.85 $R_\odot$) on the west limb, for which the electron density was measured using the inversion of Mauna Loa Solar Observatory (MLSO) coronal polarization brightness data (Cho et al. 2007, hereafter Paper I). Paper I also showed that the CME flank has a close kinematic association (speed and height) with this type II shock and gives a more favorable environment (low Alfvén speed) for coronal type II shock generation than the CME front.

The type II dynamic spectrum was obtained from the Green Bank Solar Radio Burst Spectrometer (GBSRBS). The frequency coverage of the spectrometer ranges from 18 to 70 MHz with 1 s time resolution (White et al. 2006). Since the spectrometer is located in a radio-quiet zone at NRAO's Green Bank site, it produces high-quality dynamic spectra with low-noise radio interference. The detailed description of GBSRBS and its data are available at the Web site[3] of the Green Bank observatory.

2.1. *Band Splitting*

Figure 1 shows the GBSRBS dynamic spectrum of the type II radio burst observed on 2004 August 18. This type II burst appears in two emission bands: the fundamental band that drifts from about 60 MHz at 17:44 UT to 18 MHz at 17:58 UT and the harmonic band that starts at 17:46 UT and lasts for ~40 minutes from ≥70 to 20 MHz.

[3] See http://www.nrao.edu/astrores/gbsrbs.

To distinguish the splitting branch from the harmonic bands, we followed the selection criteria proposed by Vrsnak et al. (2001). Namely, two band emission lanes should have a frequency ratio differing from 2, with more or less symmetric intensity fluctuations along the emission lanes. If they appear otherwise in frequencies with a ratio of 2, then they should be identified as the fundamental and harmonic bands.

Under this criterion, we found the band splitting in both the fundamental and the harmonic bands. Marked with dotted lines in Figure 1 are the high-frequency branch (HFB) and the lower frequency branch (LFB) of the fundamental band, which are used for the present analysis. Like other type II bursts, this type II burst also has relatively complex features; for instance, it has new band-split lanes in the harmonic band, with the HFB starting around 18:05 UT at around 40–45 MHz. However, the band-splitting structure in the considered period is relatively simple. Also note that in Figure 1 the intensity of the LFB exceeds that of the HFB. Once we accept the hypothesis that this band splitting is due to emissions from upstream and downstream, the dominance of LFB implies that the level of Langmuir turbulence in the upstream region of the shock is higher than that in the downstream region. This is consistent with theoretical considerations as well as with the 1 AU in situ measurement (e.g., Thejappa & MacDowall 2000 and references therein).

2.2. *The Coronal Density along the Shock Path*

Figure 2 shows the MK4 image (*left panel*) before the flare and CME occurred. The MLSO image allows determination of the coronal density distribution in two-dimensional space, and we need to read out the density distribution along the path of the type II bursts. In Paper I, we found that the type II burst was generated by the CME flank that interacts with the pre-existing high-density southern helmet streamer. This path is denoted as P.A. 2 in Figure 2. Although we believe that P.A. 2 is the actual path of the radio source, as described in detail in Paper I, we note that with the CME

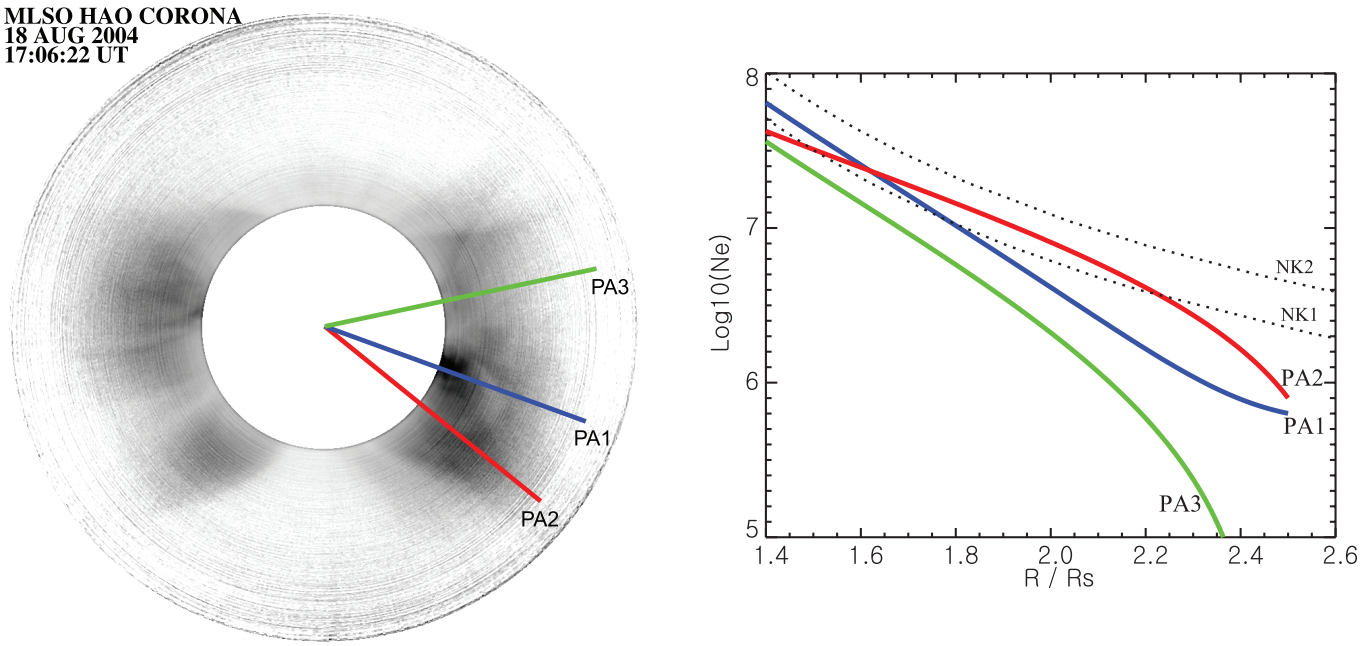

FIG. 2.—MLSO coronal polarization brightness data just before the CME events and measured density profiles along the colored lines at given position angles (P.A. 1 = 250°, P.A. 2 = 231°, and P.A. 3 = 282°). The two dotted lines labeled with NK1 and NK2 represent the one- and two-fold Newkirk density models, respectively.

image alone all position angles between P.A. 2 and P.A. 3 are potential candidates for the shock path. We will check how the spatial information of the shock will affect the diagnostic for magnetic field strength by including two other paths: along the CME nose (P.A. 1; *blue line*), and the northern streamer (P.A. 3; *green line*), although we will eventually take the result along P.A. 2 as the final result. In the right panel of Figure 2, we denote the density distribution along the CME flank (*red line*) near the southern high-density streamer (P.A. 2; *left panel*) located at the position angle of 230°, that along CME nose (*blue line*), and that along the northern streamer (*green line*), marked by P.A. 3. The inversion of polarization brightness measurement (van de Hulst 1950) was used to derive the density distribution from an average of the polarization data taken before the CME eruption.

3. THE SHOCK PROPERTIES AS A FUNCTION OF TIME

We first measure the relative instantaneous bandwidth BDW = $\triangle f/f = (f_u - f_l)/f_l$, where f_u and f_l are measured frequencies of the HFB and LFB at each moment during the type II burst. We then relate the BDW to the density jump, X, across the shock as

$$X = N_2/N_1 = (\mathrm{BDW} + 1)^2, \tag{1}$$

where N_1 and N_2 are the electron densities upstream and downstream of the shock, respectively. The density jump (X) then allows one to derive the Alfvénic Mach number (M_A) using a simplified Rankine-Hugoniot jump relation,

$$M_A = \sqrt{X(X+5)/2(4-X)}, \tag{2}$$

for perpendicular shock by assuming low plasma beta ($\beta \ll 1$) in the corona (Vrsnak et al. 2001).

We use the frequencies of the LFB and HFB of the fundamental band as marked in Figure 1 to measure the BDW and use the above equations to determine the density jump, X, and the Alfvénic Mach number (M_A) as shown in Figure 3 as a function of time, and list the numbers at selected times in Table 1. During the shock passage from 17:44 to 17:52 UT, we found that the BDW varies within the range of 0.22–0.26, which leads to a density jump varying from 1.5 to 1.6, and the Alfvénic Mach number (M_A) varies from 1.4 to 1.5. We thus notice that the Alfvénic Mach number and the density jump do not change significantly during the shock propagation. The mean values are $\langle \mathrm{BDW} \rangle = 0.24$, $\langle X \rangle = 1.54$, and $\langle M_A \rangle = 1.43$.

4. ALFVÉN SPEED PROFILE

Up to this point, we did not need the density information. We now need it in order to convert the drift of type II frequencies to the shock speed. This means that the shock path should be specified, since the density distribution along each path varies. Once the shock speed is determined, we can of course convert the Alfvén Mach number to the Alfvén speed as

$$V_A = \frac{V_{\mathrm{shock}}}{M_A}. \tag{3}$$

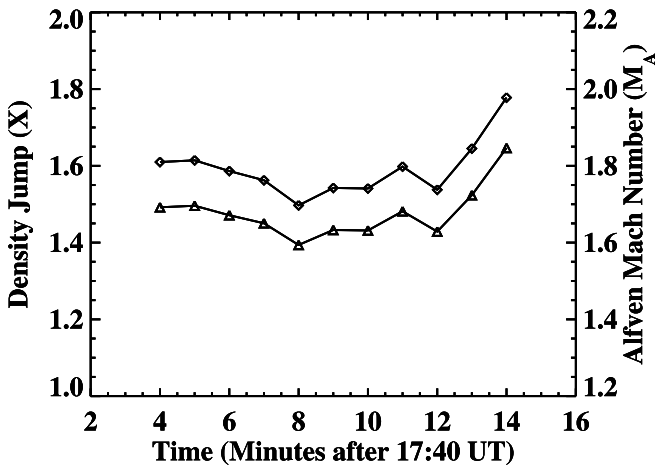

FIG. 3.—Measured density jump ratio (*top line*) and Alfvén Mach number (*bottom line*) from the band-splitting structure in the dynamic spectrum (Fig. 1).

TABLE 1
MEASUREMENT OF THE BAND SPLITTING AND DEDUCED SHOCK PARAMETERS OF THE TYPE II BURST ON 2004 AUGUST 18

Time (UT)	HFB (MHz)	LFB (MHz)	BDW	X	M_A
17:44	59	47	0.26	1.60	1.49
17:46	49	39	0.26	1.58	1.47
17:48	42	34	0.22	1.50	1.40
17:50	36	29	0.24	1.54	1.43
17:52	31	25	0.24	1.54	1.43

In Figure 4, we plot the Alfvén speed as a function of height, under the assumption that the shock passed along either P.A. 2 (*red line*), P.A. 1 (*blue line*), or P.A. 3 (*green line*). In the case of P.A. 2 (*red line*), the estimated Alfvén speed (*diamonds*) ranges from 550 to 400 km s^{-1}, with a slightly decreasing (or almost constant) value from 1.6 to 2.1 $R_\odot$. The trend of decreasing Alfvén speed in Figure 4 is similar to the result reported by Vrsnak et al. (2002), and is also comparable with the result presented by Gopalswamy et al. (2001) and Warmuth & Mann (2005). In the other cases, the inferred Alfvén speed comes out as low as ~300 km s^{-1}, while the shock traveled from 1.5 to 1.95 $R_\odot$.

As a comparison, we also show (*dotted line*) a typical model Alfvén speed constructed using the one-fold Newkirk model (Newkirk 1961) and the active region magnetic field model (Dulk & McLean 1978). We note that our result based on the density distribution along the southern streamer comes close to the typical model Alfvén speed. On the other hand, those estimated using the densities from the other regions are much lower than that of the typical model.

5. MAGNETIC FIELD

Finally, we determine the ambient magnetic field strengths using the Alfvén speed and the density in the upstream region inferred from the LFB frequencies. The field strength determined is therefore that of the yet unperturbed background field along the path of the type II shock,

$$B(\mathrm{G}) = 5.1 \times 10^{-5} f_l(\mathrm{MHz}) V_A\left(\mathrm{km\ s^{-1}}\right). \quad (4)$$

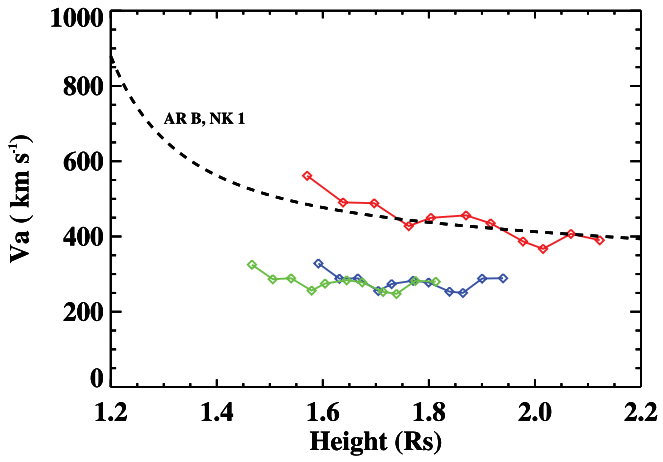

FIG. 4.—Alfvén speeds derived by using the estimated density jump from type II spectrum and coronal shock speeds from density distributions along the southern streamer (*red line*), CME nose (*blue line*), and northern streamer (*green line*). The thick dotted line indicates the deduced Alfvén speeds by using the active region magnetic field model (Dulk & McLean 1978) and one-fold Newkirk model (Newkirk 1961).

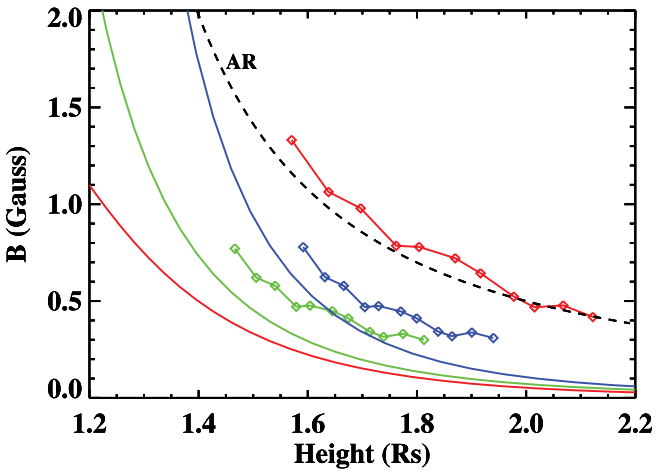

FIG. 5.—Comparisons among the coronal magnetic fields (*colored lines marked with diamonds*) derived from the type II spectrum and density measurements, the active region magnetic field model (*dotted line*), and the source surface model (*colored lines*). The same color code as that in Fig. 2 is used.

More details of the above assumptions and the analysis method are well described in Vrsnak et al. (2001).

For the purpose of comparison, we obtain the empirical active region magnetic field model and the PFSS model. The active region magnetic field model (Dulk & McLean 1978) is given by $B(R) = 0.5(R/R_\odot - 1)^{-1.5}$ G. The PFSS magnetic field model was obtained using the PFSS package available in SolarSoft.[4] As a boundary condition, this PFSS uses continually evolving full-Sun Carrington maps of the photospheric magnetic field from *SOHO* MDI full-disk magnetograms. The other boundary is, as usual, the presence of the source surface at 2.5 $R_\odot$, beyond which fields are only open and radial.

Figure 5 shows the magnetic field strength determined from the band splitting (*symbols*) in comparison with two models: Dulk & McLean's model (*dotted line*) and the PFSS model (*solid lines*). The same color code as that in Figure 2 is used here for both the band-splitting results (*symbols connected with lines*) and the PFSS model (*smooth curves*). Namely, the red, blue, and green colors correspond to the results along the position angles, P.A. 2 (the southern helmet streamer), P.A. 1 (CME nose), and P.A. 3 (the northern helmet streamer), respectively. Note that the colored symbols represent the magnetic field estimated under the assumptions on the shock path, and not all can be valid at the same time. Only those estimated along the correctly identified shock path are valid. We note that our result along P.A. 2 (*red symbols*) agrees well with the active region model, while it is much higher than the PFSS model. It is no surprise that our result comes out to be close to the empirical model of Dulk & McLean (1978), because the model employs several different techniques (e.g., optical measurement, extrapolation from photospheric magnetic field, and the solar radio burst analysis) to represent an average coronal magnetic field above active regions. Dulk & McLean (1978) state that their model fits all of the data from the different techniques to about a factor of 3, and all of our tentative results (*red, blue, and green symbols*) certainly lie within the range. However, the present technique allows us to evaluate how the magnetic field derivation is influenced by the assumed path of the type II burst source. If we had wrongly taken P.A. 1 or P.A. 3, then we would have obtained 0.3–0.8 G in the height range of 1.45–1.95 $R_\odot$. We therefore note that the values of the magnetic field determined at a given height along different

[4] See http://www.lmsal.com/solarsoft.

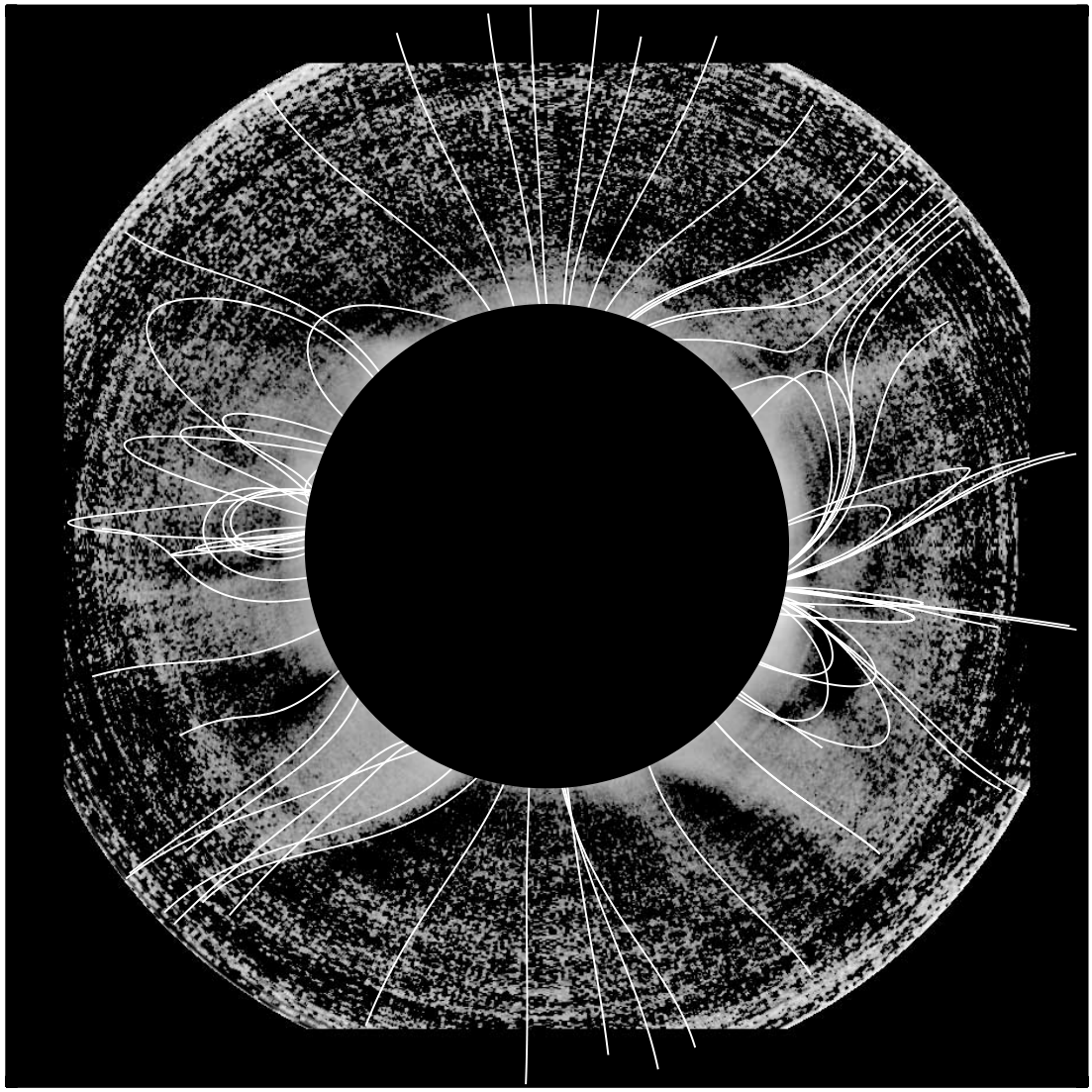

FIG. 6.—Magnetic field line configuration from the PFSS model on top of the MLSO white light image.

paths may differ by approximately a factor of 2. With independent information from Paper I on the type II source moving along P.A. 2, we can more accurately determine the magnetic field of 0.4–1.3 G in the heights 1.55–2.15 $R_{\odot}$.

To compare our result with the PFSS model, the magnetic field that we found along P.A. 2 (*red symbols*) is much higher than that predicted by the PFSS model along the same radial direction. Even though we tentatively compare the results obtained along the other two paths (*blue and green symbols*), the PFSS model predicts weaker field strength at the same locations. To further check the PFSS model, we plot in Figure 6 selected field lines from the PFSS model on top of the MLSO WL image. These field lines reproduce some of the helmet streamer structure that appears on the enhanced MLSO map. There is a general tendency that bright features on the MLSO image agree with the regions of closed field lines, and dark regions of the MLSO image correspond to the regions of open field lines in the PFSS model. We therefore consider that the PFSS model reproduces the field line topology. As a difference, our analysis shows the enhanced density and field strength near the southern streamer region, whereas this inhomogeneity cannot be included in the PFSS model. It is therefore likely that the PFSS model predicts the magnetic field topology overall, but is inherently unable to reproduce the inhomogeneity incurred by the presence of a dense streamer.

6. SUMMARY

We have analyzed the band spitting of the 2004 August 18 type II bursts to determine the coronal field strength in the range of 1.5–2.0 $R_{\odot}$. Over this height range, we found the shock compression ratio in the range of 1.5–1.6, Alfvénic Mach number, 1.4 and 1.5, Alfvén speed, 550–400 km s^{-1}, and finally the magnetic field strength, 1.3–0.6 G. In comparison, our results lie within the range (1.2–1.7) of the M_A deduced earlier for other events by Smerd et al. (1974) and Vrsnak et al. (2002). Although our result is just comparable to the range of previous band-splitting studies, one major difference of the present results from those is that we located the shock path, and identified the region to which the derived magnetic fields pertain. As we have only a single event where spatial information is given, we focused on the difference between diagnostics with or without the density and spatial information. We point out that the magnetic field strength and Alfvén velocity could be underestimated by a factor of 2 if we misidentified the shock path within the CME propagation region. When compared with the three-dimensional magnetic field provided by the PFSS

model, we found that the field strength derived from type II spectrum is higher than the model predicts. However, the field line topology predicted by the PFSS model agrees with the MLSO WL image. We thus presume that the PFSS model is capable of predicting the coronal magnetic field configuration in general, but does not find the field strength enhancement in the presence of a dense streamer along the path of the shock. We conclude that the type II band splitting provides a useful diagnostic tool for estimation of the coronal magnetic field, if the coronal density distribution is given.

We thank the anonymous referee for comments that helped to improve the manuscript. K. S. C. is indebted to R. A. Howard for help on coronal density estimation. We thank M. L. Derosa for his help with the PFSS package. K. S. C. has been supported by the MOST funds (M1-0104-00-0059 and M1-0407-00-0001) of the Korean government. J. L. was supported by NSF grant AST 06-07544 and NASA grant NNG0-6GE76G. Y. J. M. and Y. D. P. were supported by the Korea Research Foundation (KRF-2005-070-C00059) of the Korean government. The Mauna Loa Solar Observatory (MLSO) is operated by the High Altitude Observatory (HAO), a division of the National Center for Atmospheric Research (NCAR), which is sponsored by the National Science Foundation (NSF). National Radio Astronomy Observatory (NRAO) is operated for the NSF by Associated Universities, Inc., under a cooperative agreement.

REFERENCES

Cho, K.-S., Lee, J., Moon, Y.-J., Dryer, M., Bong, S.-C., Kim, Y.-H., & Park, Y.-D. 2007, A&A, 461, 1121
Cohen, M. H. 1960, ApJ, 131, 664
Dulk, G. A., & McLean, D. J. 1978, Sol. Phys., 57, 279
Gopalswamy, N., Lara, A., Kaiser, M. L., & Bougeret, J.-L. 2001, J. Geophys. Res., 106, 25261
Lee, J., White, S. M., Kundu, M. R., Mikic, Z., & McClymont, A. N. 1998, Sol. Phys., 180, 193
Lin, H., Penn, M. J., & Tomczyk, S. 2000, ApJ, 541, L83
Nelson, G. J., & Melrose, D. B. 1985, in Solar Radio Physics, ed. D. J. McLean & N. R. Labrum (Cambridge, New York), 333
Newkirk, G., Jr. 1961, ApJ, 133, 983
Schatten, K. H., Wilcox, J. M., & Ness, N. F. 1969, Sol. Phys., 6, 442
Schrijver, C. J., & DeRosa, M. L. 2003, Sol. Phys., 212, 165
Smerd, S. F., Sheridan, K. V., & Stewart, R. T. 1974, in IAU Symp. 57, ed. G. A. Newkirk, 389
Smerd, S. F., Sheridan, K. V., & Stewart, R. T. 1975, Astrophys. Lett., 16, 23
Smith, D. F. 1971, ApJ, 170, 559
Thejappa, G., & MacDowall, R. J. 2000, ApJ, 544, L163
Tidman, D. A. 1965, Planet. Space Sci., 13, 781
Tidman, D. A., Birmingham, J. J., & Stainer, H. M. 1966, ApJ, 146, 207
Van de Hulst, H. C. 1950, Bull. Astron. Inst. Netherlands, 11, 135
Vrsnak, B., Aurass, H., Magdalenic, J., & Gopalswamy, N. 2001, A&A, 377, 321
Vrsnak, B., Magdalenic, J., Aurass, H., & Mann, G. 2002, A&A, 396, 673
Warmuth, A., & Mann, G. 2005, A&A, 435, 1123
White, S. M. 2005, in Proc. International Scientific Conference on Chromospheric and Coronal Magnetic Fields, ed. D. E. Innes, A. Lagg, & S. K. Solanki (ESA SP-596; Noordwijk: ESA), 10.1
White, S. M., Bastian, T. S., Bradley, R., Parashare, C., & Wye, L. 2006, in ASP Conf. Ser. 345, From Clark Lake to the Long Wavelength Array: Bill Erickson's Radio Science, ed. N Kassim et al. (San Francisco: ASP), 176